INTERNATIONAL JOURNAL FOR NUMERICAL METHODS IN FLUIDS
Int. J. Numer. Meth. Fluids 2007; **55**:41–56
Published online 31 January 2007 in Wiley InterScience (www.interscience.wiley.com). DOI: 10.1002/fld.1440

A multi-energy-level lattice Boltzmann model for the compressible Navier–Stokes equations

Guangwu Yan*,†, Jianying Zhang, Yanhong Liu and Yinfeng Dong

College of Mathematics, Jilin University, Changchun 130012, People's Republic of China

SUMMARY

In this paper, we propose a new lattice Boltzmann model for the compressible Navier–Stokes equations. The new model is based on a three-energy-level and three-speed lattice Boltzmann equation by using a method of higher moments of the equilibrium distribution functions. As the 25-bit model, we obtained the equilibrium distribution functions and the compressible Navier–Stokes equations with the second accuracy of the truncation errors. The numerical examples show that the model can be used to simulate the shock waves, contact discontinuities and supersonic flows around circular cylinder. The numerical results are compared with those obtained by traditional method. Copyright © 2007 John Wiley & Sons, Ltd.

Received 7 May 2006; Revised 5 December 2006; Accepted 6 December 2006

KEY WORDS: lattice Boltzmann method; compressible Navier–Stokes equations; Sod's problem

1. INTRODUCTION

Recently, the lattice Boltzmann method (LBM) has been developed as an alternative method for computational fluid dynamics (CFD). This method originated from a Boolean fluid model known as the lattice gas automata (LGA) [1, 2] which simulates the motion of the fluids by particles moving and colliding on a regular lattice. During the past few years much progress has been made that extend the LBM to become a tool for simulating many complex fluid dynamics problems, such as multi-phase flow, suspension flow and flow in the porous media, which are quite difficult to simulate by conventional method. All of LBMs approach computation; the famous lattice Bhatnagar–Gross–Krook (LBGK) scheme is simple and the most recent application to attract interest [2].

*Correspondence to: Guangwu Yan, College of Mathematics, Jilin University, Changchun 130012, People's Republic of China.
†E-mail: yangw@email.jlu.edu.cn

Contract/grant sponsor: National Nature Science Foundation of China; contract/grant numbers: 10072023, 90305013
Contract/grant sponsor: Chuangxin Foundation of Jilin University; contract/grant number: 2004CX041

Unlike conventional methods based on macroscopic continuum equation, the LBGK starts from mesoscopic kinetic equations, i.e. the Boltzmann equation, to determine the macroscopic fluid flows. The kinetic nature offers certain advantages over conventional numerical methods, such as their algorithmic simplicity, parallel computation, easy handling of complex boundary conditions and efficient hydrodynamics simulations [3–5]. A recent study by Yan *et al.* showed that the LBGK model could be used to simulate wave motion [6], soliton wave [7], and Lorenz attractor [8]; all these models can be derived by using higher-order moment method with multi-scale technique. Now, we focus on the compressible Navier–Stokes equation and propose a new model with higher-order moment method for simulating wave and contact discontinuity.

There are many significant refined finite-difference methods for the compressible flows in history [9–14]. For example, the finite volume method with unstructured meshes is to fit complex boundaries [9]; the total variation diminishing (TVD) [10]; the essentially non-oscillatory (ENO) [11] methods are to minimize numerical diffusions and non-physical oscillatory effects; the meshless method can avoid the restriction of grid meshes [12]. The level set method can be used to trace the moving boundaries [13]. When these schemes are applied to a shock wave tube problem, they produce a very high resolution for the shock, especially in TVD-type schemes. However, the contact discontinuity is still spread over typically three to four grid cells. For Eulerian finite-difference method, contact discontinuities are more difficult to compute with high resolution than in the case of shock since they do not have a natural compression mechanism to help their sharp numerical resolution. The LBM can offer an ideal numerical effect and a new insight [15].

It is known that the LBM is limited to the low Mach flows [15], although several related compressible techniques have been proposed. In order to remove the low Mach restriction, in recent years, a series of LBM for the compressible flows has been proposed [16–30]. Alexander *et al.* [16] chose a modified equilibrium distribution, allowing the sound speed to be small. Nadiga [17] proposed a discrete velocity model. Huang *et al.* [18] used flow-adapted discrete velocities, a non-unique equilibrium distribution constrained by a set of linear moments and the used interpolated nodes. Prendergast and Xu [19], Kim *et al.* [20] and Koltelnikov and Montgomery used Bhatnagar–Gross–Krook-type models [21] to establish new type flux and employed TVD flux limitation with the neighbourhood cells. Renda *et al.* [22], Vahala *et al.* [23], Sun [24], De Cicco *et al.* [25], Mason [26, 27], Yan [15, 28], and Kataoka and Tsutahara [29, 30] proposed many models by using additional techniques to achieve higher Mach number for the compressible flows.

The earlier LBMs encounter two difficulties which need to be solved: (1) the accuracy of these models is first-order system; (2) the equilibrium distribution functions, the higher moments are not unknown. In his paper, to overcome these problems, we propose a new two-dimensional model. In comparison with the earlier LBM, the third moment P_{ijk} and moment R_{ij} have been added to fit the macroscopic equations, say, the compressible Navier–Stokes equations with the second-order model. Therefore, we would obtain the equilibrium distribution functions. One-dimensional model may not be a suitable one for simulating one-dimensional compressible flows, because there is no correspondence between the first-order one-dimensional model and the compressible flows. Therefore, we focus our attention on the two-dimensional model. Our goal is to build a lattice Boltzmann model with the second-order model for the compressible Navier–Stokes equations.

The new model is based on a three-energy-level and three-speed lattice Boltzmann equation by using a method of higher moments of the equilibrium distribution functions [6]. As the 25-bit model, we obtained the equilibrium distribution functions and the compressible Navier–Stokes equations with the second-order accuracy of the truncation errors. The numerical examples show that the model can be used to simulate the shock waves, contact discontinuities and supersonic flows

DOI: 10.1002/fld

around circular cylinder. The numerical results are compared with those obtained by traditional method.

In the next section, the second-order LBM is described. In Section 3, we simulate two numerical examples with shock waves and contact discontinuities, and Section 4 gives concluding remarks.

2. LATTICE BOLTZMANN MODEL

2.1. Lattice Boltzmann equation

We consider a two-layer hexagon lattice with 12 links that connect the centre site to 12 neighbour nodes. We assume that the particles moving along the link with velocity $\mathbf{e}_\alpha$ are divided into two kinds, A and B, with different energy levels ε_A ($\alpha = 1, \ldots, 12$) and ε_B ($\alpha = 13, \ldots, 24$), and the rest particles ($\alpha = 0$) possess energy level ε_D. So it is actually a 25-bit model with three speeds 0, c and $2c$, where c is the speed of particles at the face centres: $|e_\alpha| = c$ ($\alpha = 1, \ldots, 6$ and $\alpha = 13, \ldots, 18$), $|e_\alpha| = 2c$ ($\alpha = 7, \ldots, 12$ and $\alpha = 19, \ldots, 24$) and $|e_0| = 0$, see Figure 1.

We define $f_\alpha(\mathbf{x}, t)$ as the distribution function at site x and time t, with velocity $\mathbf{e}_\alpha$. The macroscopic quantity mass, momentum and total energy per site are defined as follows:

$$\rho = \sum_\alpha f_\alpha \tag{1}$$

$$\rho u_j = \sum_\alpha e_{\alpha j} f_\alpha \tag{2}$$

$$\frac{1}{2}\rho u^2 + \rho E = \sum_\alpha f_\alpha \varepsilon_\alpha \tag{3}$$

in Equation (3), E is the internal energy per unit mass. The ε_α is the energy level [15], it has only three numerical values, ε_A, ε_B, and ε_D. The lattice Boltzmann equations are expressed as

$$f_\alpha(\mathbf{x} + \mathbf{e}_\alpha, t + 1) = f_\alpha(\mathbf{x}, t) - \frac{1}{\tau}(f_\alpha(\mathbf{x}, t) - f_\alpha^{\mathrm{eq}}(\mathbf{x}, t)) \tag{4}$$

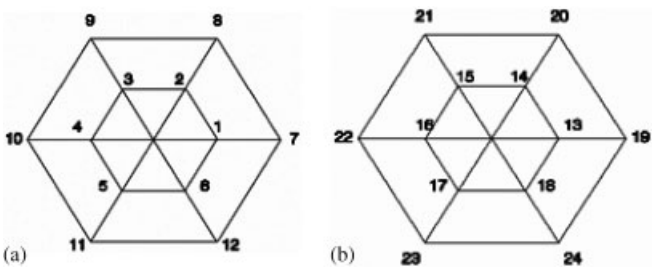

Figure 1. Schematic diagram of lattice: (a) type A and (b) type B.

DOI: 10.1002/fld

where τ is the single-relaxation time, $f_\alpha^{\mathrm{eq}}(\mathbf{x}, t)$ is the local equilibrium distribution function at site $\mathbf{x}$ and time t, with velocity $\mathbf{e}_\alpha$. We assume that f_α^{eq} has the following form:

$$f_\alpha^{\mathrm{eq}} = A_0'\rho + A_2'\rho u_j e_{\alpha j} + A_5'\rho u_i u_j e_{\alpha i} e_{\alpha j} + A_6'\rho u^2 + A_7'\rho u_i u_j u_k e_{\alpha i} e_{\alpha j} e_{\alpha k}$$
$$(\alpha = 1, \ldots, 6), \quad \varepsilon_\alpha = \varepsilon_A$$

$$f_\alpha^{\mathrm{eq}} = A_0''\rho + A_2''\rho u_j e_{\alpha j} + A_5''\rho u_i u_j e_{\alpha i} e_{\alpha j} + A_6''\rho u^2 + A_7''\rho u_i u_j u_k e_{\alpha i} e_{\alpha j} e_{\alpha k}$$
$$(\alpha = 7, \ldots, 12), \quad \varepsilon_\alpha = \varepsilon_A$$

$$f_\alpha^{\mathrm{eq}} = B_0'\rho + B_2'\rho u_j e_{\alpha j} + B_5'\rho u_i u_j e_{\alpha i} e_{\alpha j} + B_6'\rho u^2 + B_7'\rho u_i u_j u_k e_{\alpha i} e_{\alpha j} e_{\alpha k}$$
$$(\alpha = 13, \ldots, 18), \quad \varepsilon_\alpha = \varepsilon_B$$

$$f_\alpha^{\mathrm{eq}} = B_0''\rho + B_2''\rho u_j e_{\alpha j} + B_5''\rho u_i u_j e_{\alpha i} e_{\alpha j} + B_6''\rho u^2 + B_7''\rho u_i u_j u_k e_{\alpha i} e_{\alpha j} e_{\alpha k}$$
$$(\alpha = 19, \ldots, 24), \quad \varepsilon_\alpha = \varepsilon_B$$

$$f_0^{\mathrm{eq}} = D_0\rho + D_6\rho u^2 \quad (\alpha = 0), \quad \varepsilon_\alpha = \varepsilon_D$$

where coefficients A_β', A_β'', B_β', B_β'' ($\beta = 0,\ 2,\ 5,\ 6,\ 7$), and D_β ($\beta = 0,\ 6$) are determined by a set of reasonable requirements. These requirements consist of the conservation laws of mass, momentum, energy and the conditions of higher-order moment [31]

$$\sum_\alpha f_\alpha^{\mathrm{eq}} = \rho \tag{5}$$

$$\sum_\alpha f_\alpha^{\mathrm{eq}} e_{\alpha j} = \rho u_j \tag{6}$$

$$\sum_\alpha f_\alpha^{\mathrm{eq}} \varepsilon_\alpha = \frac{1}{2}\rho u^2 + \rho E \tag{7}$$

$$\pi_{ij}^0 \equiv \sum_\alpha f_\alpha^{\mathrm{eq}} e_{\alpha i} e_{\alpha j} = \rho u_i u_j + p\delta_{ij} \tag{8}$$

$$Q_j^0 \equiv \sum_\alpha f_\alpha^{\mathrm{eq}} e_{\alpha j} \varepsilon_\alpha = \left(\frac{1}{2}\rho u^2 + \rho E + p\right) u_j \tag{9}$$

$$P_{ijk}^0 \equiv \sum_\alpha f_\alpha^{\mathrm{eq}} e_{\alpha i} e_{\alpha j} e_{\alpha k} = \rho u_i u_j u_k + p u_k \delta_{ij} + p\delta_{ik} u_j + p\delta_{jk} u_i \tag{10}$$

$$R_{jk}^0 \equiv \sum_\alpha f_\alpha^{\mathrm{eq}} e_{\alpha j} e_{\alpha k} \varepsilon_\alpha$$
$$= \frac{1}{2}\rho u^2 u_j u_k + (2\gamma - 1)\rho E u_j u_k + \frac{1}{2}(\gamma - 1)\rho u^2 E\delta_{jk} + (\gamma - 1)\gamma\rho E^2\delta_{jk} \tag{11}$$

DOI: 10.1002/fld

where p is the pressure of the perfect gas

$$p = (\gamma - 1)\rho E \tag{12}$$

γ is the specific-heat ratio.

2.2. *Coefficients in the equilibrium distribution*

The form of the Navier–Stokes equation depends on few specific properties of the hexagonal lattice model. The most important properties relate to the symmetries of the moments

$$T^n_{i_1,\ldots,i_n} = \sum_{\alpha} e_{\alpha i_1} \ldots e_{\alpha i_n} \tag{13}$$

In this paper, moments $T^1, \ldots, T^6$ are used, according to Reference [32], we get

$$T^2_{ij} = \frac{bc^2}{D}\delta_{ij} \tag{14}$$

$$T^4_{ijkm} = \frac{bc^4}{D(D+2)}\Delta^4_{ijkm} \tag{15}$$

where $\Delta^4_{ijkm} = \delta_{ij}\delta_{km} + \delta_{ik}\delta_{jm} + \delta_{im}\delta_{jk}$.

$$T^6_{ijklmn} = \frac{bc^6}{D(D+2)(D+4)}\Delta^6_{ijklmn} \tag{16}$$

$$\begin{aligned}\Delta^6_{ijklmn} = {} & \delta_{ij}\Delta_{klmn} + \delta_{ik}\Delta_{jlmn} + \delta_{il}\Delta_{jkmn} + \delta_{im}\Delta_{jk\,\ln} + \delta_{in}\Delta_{jklm} \\ & + \delta_{jk}\Delta_{ilmn} + \delta_{jl}\Delta_{ikmn} + \delta_{jm}\Delta_{ik\,\ln} + \delta_{jn}\Delta_{iklm} + \delta_{kl}\Delta_{ijmn} \\ & + \delta_{km}\Delta_{ij\,\ln} + \delta_{kn}\Delta_{ijlm} + \delta_{lm}\Delta_{ijkn} + \delta_{\ln}\Delta_{ijkm} + \delta_{mn}\Delta_{ijkl}\end{aligned} \tag{17}$$

Therefore,

$$\Delta_{ijklmn}\rho u_l u_m u_n = 18\rho u_i u_j u_k + 9\rho u^2 u_k \delta_{ij} + 9\rho u^2 u_j \delta_{ik} + 9\rho u^2 u_i \delta_{jk} \tag{18}$$

Substituting equilibrium distribution function into (5)–(11) and using the identity equations (14)–(18), we obtain the system of linear equations for determining the following equation of coefficients A'_β, A''_β, B'_β, B''_β ($\beta = 0,\ 2,\ 5,\ 6,\ 7$), and $D_\beta (\beta = 0, 6)$

$$b(A'_0 + A''_0 + B'_0 + B''_0) + D_0 = 1 \tag{19}$$

$$\frac{b}{D}(A'_5 c_1^2 + A''_5 c_2^2 + B'_5 c_1^2 + B''_5 c_2^2) + b(A'_6 + A''_6 + B'_6 + B''_6) + D_6 = 0 \tag{20}$$

$$\frac{b}{D}(A'_2 c_1^2 + A''_2 c_2^2 + B'_2 c_1^2 + B''_2 c_2^2) = 1 \tag{21}$$

$$\frac{b}{D(D+2)}(A'_7 c_1^4 + A''_7 c_2^4 + B'_7 c_1^4 + B''_7 c_2^4) = 0 \tag{22}$$

DOI: 10.1002/fld

$$b(A'_0\varepsilon_A + A''_0\varepsilon_A + B'_0\varepsilon_B + B''_0\varepsilon_B) + D_0\varepsilon_D = E \tag{23}$$

$$\frac{b}{D}(A'_5\varepsilon_A c_1^2 + A''_5\varepsilon_A c_2^2 + B'_5\varepsilon_B c_1^2 + B''_5\varepsilon_B c_2^2) + b(A'_6\varepsilon_A + A''_6\varepsilon_A + B'_6\varepsilon_B + B''_6\varepsilon_B) + D_6\varepsilon_D = \frac{1}{2} \tag{24}$$

$$\frac{\rho b}{D}(A'_0 c_1^2 + A''_0 c_2^2 + B'_0 c_1^2 + B''_0 c_2^2) = p \tag{25}$$

$$\frac{2b}{D(D+2)}(A'_5 c_1^4 + A''_5 c_2^4 + B'_5 c_1^4 + B''_5 c_2^4) = 1 \tag{26}$$

$$\frac{b}{D}(A_6^1 c_1^2 + A''_6 c_2^2 + B_6^1 c_1^2 + B'_6 c_2^2) + \frac{b}{D(D+2)}(A'_5 c_1^4 + A''_5 c_2^4 + B'_5 c_1^4 + B''_5 c_2^4) = 0 \tag{27}$$

$$\frac{b}{D}(A'_2\varepsilon_A c_1^2 + A''_2\varepsilon_A c_2^2 + B'_2\varepsilon_B c_1^2 + B''_2\varepsilon_B c_2^2) = \gamma E \tag{28}$$

$$\frac{3b}{D(D+2)}(A'_7\varepsilon_A c_1^4 + A''_7\varepsilon_A c_2^4 + B'_7\varepsilon_B c_1^4 + B''_7\varepsilon_B c_2^4) = \frac{1}{2} \tag{29}$$

$$\frac{b}{D(D+2)}(A'_2 c_1^4 + A''_2 c_2^4 + B'_2 c_1^4 + B''_2 c_2^4) + \frac{9bu^2}{D(D+2)(D+4)}(A'_7 c_1^6 + A''_7 c_2^6 + B'_7 c_1^6 + B''_7 c_2^6) = (\gamma - 1)E \tag{30}$$

$$\frac{18b}{D(D+2)(D+4)}(A'_7 c_1^6 + A''_7 c_2^6 + B'_7 c_1^6 + B''_7 c_2^6) = 1 \tag{31}$$

$$\frac{b}{D}(A'_0\varepsilon_A c_1^2 + A''_0\varepsilon_A c_2^2 + B'_0\varepsilon_B c_1^2 + B''_0\varepsilon_B c_2^2) = \gamma(\gamma - 1)E^2 \tag{32}$$

$$\frac{2b}{D(D+2)}(A'_5\varepsilon_A c_1^4 + A''_5\varepsilon_A c_2^4 + B'_5\varepsilon_B c_1^4 + B''_5\varepsilon_B c_2^4) = \frac{1}{2}u^2 + (2\gamma - 1)E \tag{33}$$

$$\frac{b}{D}(A'_6\varepsilon_A c_1^2 + A''_6\varepsilon_A c_2^2 + B'_6\varepsilon_B c_1^2 + B''_6\varepsilon_B c_2^2) + \frac{b}{D(D+2)}(A'_5 c_1^4\varepsilon_A + A''_5 c_2^4\varepsilon_A + B'_5 c_1^4\varepsilon_B + B''_5 c_2^4\varepsilon_B) = \frac{1}{2}(\gamma - 1)E \tag{34}$$

here, D ($=2$) is the space dimension and b ($=6$, for hexagonal lattice) is the link number per site.

In order to obtain these coefficients in the equilibrium distribution, we have to propose some man-made complementary conditions. We introduce the following assumptions:

$$A'_0\varepsilon_A + B'_0\varepsilon_B = 4(A''_0\varepsilon_A + B''_0\varepsilon_B) = \frac{\gamma(\gamma - 1)E^2 D}{2bc^2} \tag{35}$$

DOI: 10.1002/fld

$$A_2'\varepsilon_A + B_2'\varepsilon_B = 4(A_2''\varepsilon_A + B_2''\varepsilon_B) = \frac{D\gamma E}{2bc^2} \tag{36}$$

$$A_5' + B_5' = 16(A_5'' + B_5'') = \frac{D(D+2)}{4bc^4} \tag{37}$$

$$A_6' + B_6' = 4(A_6'' + B_6'') = -\frac{D}{4bc^2} \tag{38}$$

$$A_6'\varepsilon_A + B_6'\varepsilon_B = 4(A_6''\varepsilon_A + B_6''\varepsilon_B) = -\frac{D(\gamma E + 0.5u^2)}{4bc^2} \tag{39}$$

$$A_7'\varepsilon_A + B_7'\varepsilon_B = 16(A_7''\varepsilon_A + B_7''\varepsilon_B) = \frac{D(D+2)}{12bc^4} \tag{40}$$

Thus, we have

$$A_0' = \frac{1}{\varepsilon_A - \varepsilon_B}\left\{\frac{\gamma(\gamma-1)E^2D}{2bc^2} + \frac{\varepsilon_B pD}{3\rho bc^2} - \frac{4\varepsilon_B}{3b} + \frac{4\varepsilon_B}{3b\varepsilon_D}\left[E - \frac{5\gamma(\gamma-1)E^2D}{8c^2}\right]\right\} \tag{41}$$

$$B_0' = \frac{1}{\varepsilon_A - \varepsilon_B}\left\{-\frac{\gamma(\gamma-1)E^2D}{2bc^2} - \frac{\varepsilon_A pD}{3\rho bc^2} + \frac{4\varepsilon_A}{3b} - \frac{4\varepsilon_A}{3b\varepsilon_D}\left[E - \frac{5\gamma(\gamma-1)E^2D}{8c^2}\right]\right\} \tag{42}$$

$$A_0'' = \frac{1}{\varepsilon_A - \varepsilon_B}\left\{\frac{\gamma(\gamma-1)E^2D}{8bc^2} - \frac{\varepsilon_B pD}{3\rho bc^2} + \frac{\varepsilon_B}{3b} - \frac{\varepsilon_B}{3b\varepsilon_D}\left[E - \frac{5\gamma(\gamma-1)E^2D}{8c^2}\right]\right\} \tag{43}$$

$$B_0'' = \frac{1}{\varepsilon_A - \varepsilon_B}\left\{-\frac{\gamma(\gamma-1)E^2D}{8bc^2} + \frac{\varepsilon_A pD}{3\rho bc^2} - \frac{\varepsilon_A}{3b} + \frac{\varepsilon_A}{3b\varepsilon_D}\left[E - \frac{5\gamma(\gamma-1)E^2D}{8c^2}\right]\right\} \tag{44}$$

$$D_0 = \left[E - \frac{5}{c^2}\gamma(\gamma-1)E^2D\right]\frac{1}{\varepsilon_D} \tag{45}$$

$$A_2' = \frac{1}{\varepsilon_A - \varepsilon_B}\left\{\frac{D\gamma E}{2bc^2} - \frac{4D\varepsilon_B}{3bc^2} + \frac{D(D+2)\varepsilon_B}{3bc^4}\left[(\gamma-1)E - \frac{1}{2}u^2\right]\right\} \tag{46}$$

$$B_2' = \frac{1}{\varepsilon_A - \varepsilon_B}\left\{-\frac{D\gamma E}{2bc^2} + \frac{4D\varepsilon_A}{3bc^2} - \frac{D(D+2)\varepsilon_A}{3bc^4}\left[(\gamma-1)E - \frac{1}{2}u^2\right]\right\} \tag{47}$$

$$A_2'' = \frac{1}{\varepsilon_A - \varepsilon_B}\left\{\frac{D\gamma E}{8bc^2} - \frac{\varepsilon_B D(D+2)}{12bc^4}\left[(\gamma-1)E - \frac{1}{2}u^2\right] + \frac{D\varepsilon_B}{12bc^2}\right\} \tag{48}$$

$$B_2'' = \frac{1}{\varepsilon_A - \varepsilon_B}\left\{-\frac{D\gamma E}{8bc^2} + \frac{\varepsilon_A D(D+2)}{12bc^4}\left[(\gamma-1)E - \frac{1}{2}u^2\right] - \frac{D\varepsilon_A}{12bc^2}\right\} \tag{49}$$

$$A_5' = \frac{1}{\varepsilon_A - \varepsilon_B}\left\{\frac{2D}{3bc^2} + \frac{10D\varepsilon_D}{12bc^4} + \frac{5D^2}{12bc^4}\left(\frac{1}{2}u^2 + \gamma E\right) - \frac{D(D+2)}{6bc^4}\left[\frac{1}{2}u^2 + (2\gamma-1)E\right] - \frac{\varepsilon_B D(D+2)}{4bc^4}\right\} \tag{50}$$

DOI: 10.1002/fld

$$B_5' = \frac{1}{\varepsilon_A - \varepsilon_B}\left\{-\frac{2D}{3bc^2} - \frac{10D\varepsilon_D}{12bc^4} - \frac{5D^2}{12bc^4}\left(\frac{1}{2}u^2 + \gamma E\right) + \frac{D(D+2)}{6bc^4}\left[\frac{1}{2}u^2 + (2\gamma - 1)E\right] + \frac{\varepsilon_A D(D+2)}{4bc^4}\right\} \tag{51}$$

$$A_5'' = \frac{1}{\varepsilon_A - \varepsilon_B}\left\{\frac{D(D+2)}{24bc^4}\left[\frac{1}{2}u^2 + (2\gamma - 1)E\right] + \frac{1}{12}\left[-\frac{D}{2bc^2} - \frac{10D\varepsilon_D}{16bc^4} - \frac{5D^2}{16bc^4}\left(\frac{1}{2}u^2 + \gamma E\right)\right] - \varepsilon_B \frac{D(D+2)}{64bc^4}\right\} \tag{52}$$

$$B_5'' = \frac{1}{\varepsilon_A - \varepsilon_B}\left\{-\frac{D(D+2)}{24bc^4}\left[\frac{1}{2}u^2 + (2\gamma - 1)E\right] - \frac{1}{12}\left[-\frac{D}{2bc^2} - \frac{10D\varepsilon_D}{16bc^4} - \frac{5D^2}{16bc^4}\left(\frac{1}{2}u^2 + \gamma E\right)\right] + \varepsilon_A \frac{D(D+2)}{64bc^4}\right\} \tag{53}$$

$$A_6' = \frac{1}{\varepsilon_A - \varepsilon_B}\left\{-\frac{D}{4bc^2}\left(\gamma E + \frac{1}{2}u^2\right) + \frac{D\varepsilon_B}{4bc^2}\right\} \tag{54}$$

$$B_6' = \frac{1}{\varepsilon_A - \varepsilon_B}\left\{\frac{D}{4bc^2}\left(\gamma E + \frac{1}{2}u^2\right) - \frac{D\varepsilon_A}{4bc^2}\right\} \tag{55}$$

$$A_6'' = \frac{1}{\varepsilon_A - \varepsilon_B}\left\{-\frac{D}{16bc^2}\left(\frac{1}{2}u^2 + \gamma E\right) + \frac{D\varepsilon_B}{16bc^2}\right\} \tag{56}$$

$$B_6'' = \frac{1}{\varepsilon_A - \varepsilon_B}\left\{\frac{D}{16bc^2}\left(\frac{1}{2}u^2 + \gamma E\right) - \frac{D\varepsilon_A}{16bc^2}\right\} \tag{57}$$

$$D_6 = -\frac{10}{16c^2} \tag{58}$$

$$A_7' = \frac{1}{\varepsilon_A - \varepsilon_B}\left[\frac{D(D+2)}{12bc^4} + \frac{D(D+2)(D+4)\varepsilon_B}{54bc^6}\right] \tag{59}$$

$$B_7' = \frac{1}{\varepsilon_A - \varepsilon_B}\left[-\frac{D(D+2)}{12bc^4} - \frac{D(D+2)(D+4)\varepsilon_A}{54bc^6}\right] \tag{60}$$

$$A_7'' = \frac{1}{\varepsilon_A - \varepsilon_B}\left[\frac{D(D+2)}{192bc^4} - \frac{D(D+2)(D+4)\varepsilon_B}{864bc^6}\right] \tag{61}$$

$$B_7'' = \frac{1}{\varepsilon_A - \varepsilon_B}\left[-\frac{D(D+2)}{192bc^4} + \frac{D(D+2)(D+4)\varepsilon_A}{864bc^6}\right] \tag{62}$$

DOI: 10.1002/fld

2.3. Macroscopic equations

Using a small parameter k as the time step in numerical simulation, we take that it equals the Knudsen number [6]. The lattice Boltzmann equation in physical unit is

$$f_\alpha(\mathbf{x}+ke_\alpha, t+k) - f_\alpha(\mathbf{x}, t) = -\frac{1}{\tau}(f_\alpha(\mathbf{x}, t) - f_\alpha^{\mathrm{eq}}(\mathbf{x}, t)) \tag{63}$$

The Chapman–Enskog expansion [33] is applied to $f_\alpha(\mathbf{x}, t)$ under the assumption that the small Knudsen number

$$f_\alpha = \sum_{n=0}^{\infty} k^n f_\alpha^n = f_\alpha^0 + k f_\alpha^1 + k^2 f_\alpha^2 + \cdots + \tag{64}$$

where f_α^0 denotes f_α^{eq}. We discuss changes in different time scales, introduced as $t_0, t_1, \ldots$, thus,

$$t_0 = t, \quad t_1 = kt, \quad t_2 = k^2 t, \quad t_3 = k^3 t, \ldots$$

and

$$\frac{\partial}{\partial t} = \frac{\partial}{\partial t_0} + k\frac{\partial}{\partial t_1} + k^2\frac{\partial}{\partial t_2} + k^3\frac{\partial}{\partial t_3} + O(k^2) \tag{65}$$

Performing the Taylor expansion using Equation (63), and retaining terms up to $O(k^3)$, we obtain a series of lattice Boltzmann equations in different time t_0, t_1, t_2 scales [6]

$$\frac{\partial f_\alpha^{\mathrm{eq}}}{\partial t_0} + e_{\alpha j}\frac{\partial f_\alpha^{\mathrm{eq}}}{\partial x_j} = -\frac{1}{\tau} f_\alpha^1 \tag{66}$$

$$\frac{\partial f_\alpha^{\mathrm{eq}}}{\partial t_1} + \left(\frac{1}{2} - \tau\right)\left(\frac{\partial}{\partial t_0} + e_{\alpha j}\frac{\partial}{\partial x_j}\right)^2 f_\alpha^{\mathrm{eq}} = -\frac{1}{\tau} f_\alpha^2 \tag{67}$$

$$\begin{aligned}&\frac{\partial f_\alpha^{\mathrm{eq}}}{\partial t_2} + (1-2\tau)\left(\frac{\partial}{\partial t_0} + e_{\alpha j}\frac{\partial}{\partial x_j}\right)\frac{\partial f_\alpha^{\mathrm{eq}}}{\partial t_1} + \left(\tau^2 - \tau + \frac{1}{6}\right)\left(\frac{\partial}{\partial t_0} + e_{\alpha j}\frac{\partial}{\partial x_j}\right)^3 f_\alpha^{\mathrm{eq}} \\ &\quad = -\frac{1}{\tau} f_\alpha^3\end{aligned} \tag{68}$$

We obtain the conversation laws in the first time scale t_0 easily

$$\frac{\partial \rho}{\partial t_0} + \frac{\partial \rho u_j}{\partial x_j} = 0 \tag{69}$$

$$\frac{\partial \rho u_i}{\partial t_0} + \frac{\partial \pi_{ij}^0}{\partial x_j} = 0 \tag{70}$$

$$\frac{\partial(\frac{1}{2}\rho u^2 + \rho E)}{\partial t_0} + \frac{\partial Q_j^0}{\partial x_j} = 0 \tag{71}$$

DOI: 10.1002/fld

and the Navier–Stokes equations with the two-order accuracy

$$\frac{\partial \rho}{\partial t} + \frac{\partial \rho u_j}{\partial x_j} = O(k^2) \tag{72}$$

$$\frac{\partial \rho u_i}{\partial t} + \frac{\partial \pi_{ij}^0}{\partial x_j} = \frac{\partial}{\partial x_k}\left[\xi\left(\frac{\partial u_i}{\partial x_k} + \frac{\partial u_k}{\partial x_i}\right) - \eta \frac{\partial u_j}{\partial x_j}\delta_{ik}\right] + O(k^2) \tag{73}$$

$$\frac{\partial(\frac{1}{2}\rho u^2 + \rho E)}{\partial t} + \frac{\partial Q_j^0}{\partial x_j} = \frac{\partial}{\partial x_j}\left[\zeta \frac{\partial E}{\partial x_j} + u_k \xi\left(\frac{\partial u_k}{\partial x_j} + \frac{\partial u_j}{\partial x_k}\right) - u_k \eta \frac{\partial u_m}{\partial x_m}\delta_{jk}\right] + O(k^2) \tag{74}$$

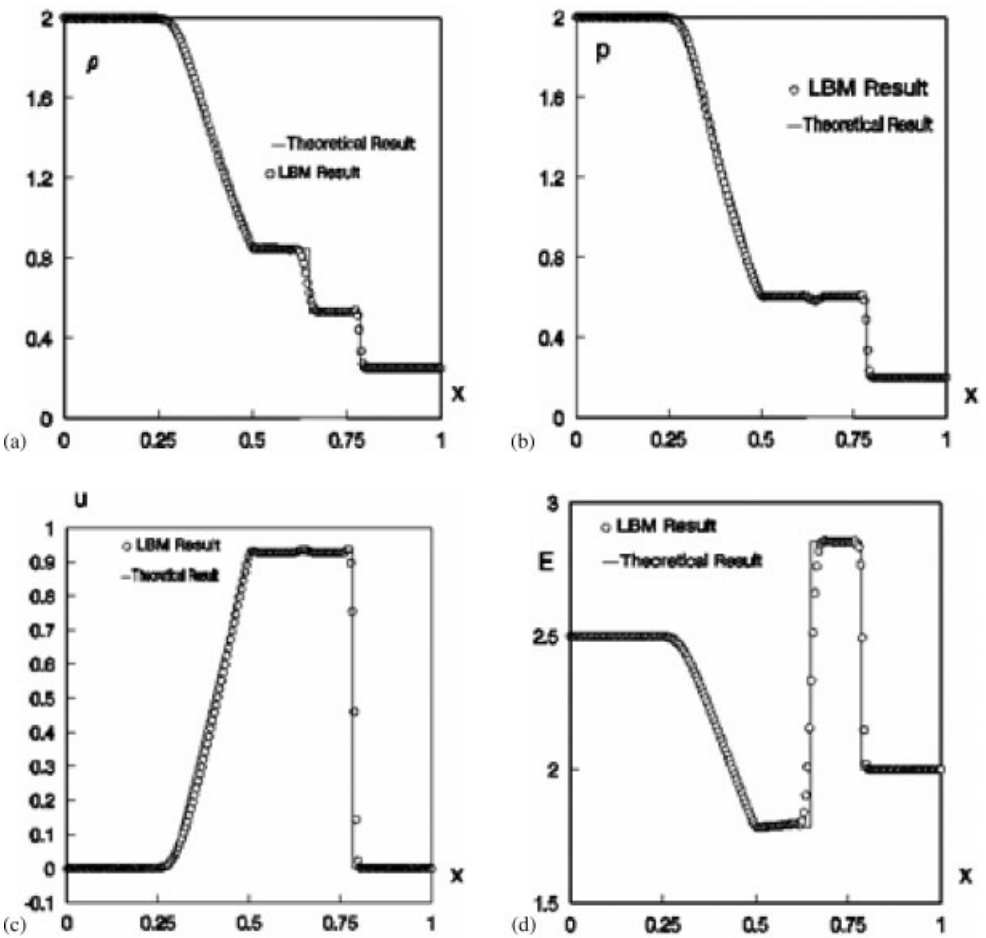

Figure 2. Comparison of exact solution and one-order LBM results of one-dimensional Sod's problem: (a)–(d) (solid lines are exact solutions, circles are LBM results): (a) density; (b) pressure; (c) velocity; and (d) internal energy. Parameters: $\gamma = 1.4$, $c = 3.0$, $\tau = 1.51$, $\varepsilon_A = 2c^2$, $\varepsilon_B = 0.6c^2$, $\varepsilon_D = 0.13c^2$, lattice size 200×4, time $t = 100\Delta t$.

DOI: 10.1002/fld

where

$$\xi = k(\tau - \tfrac{1}{2})(\gamma - 1)\rho E \tag{75}$$

$$\eta = k(\tau - \tfrac{1}{2})(\gamma - 1)^2 \rho E \tag{76}$$

$$\zeta = k(\tau - \tfrac{1}{2})\gamma(\gamma - 1)\rho E \tag{77}$$

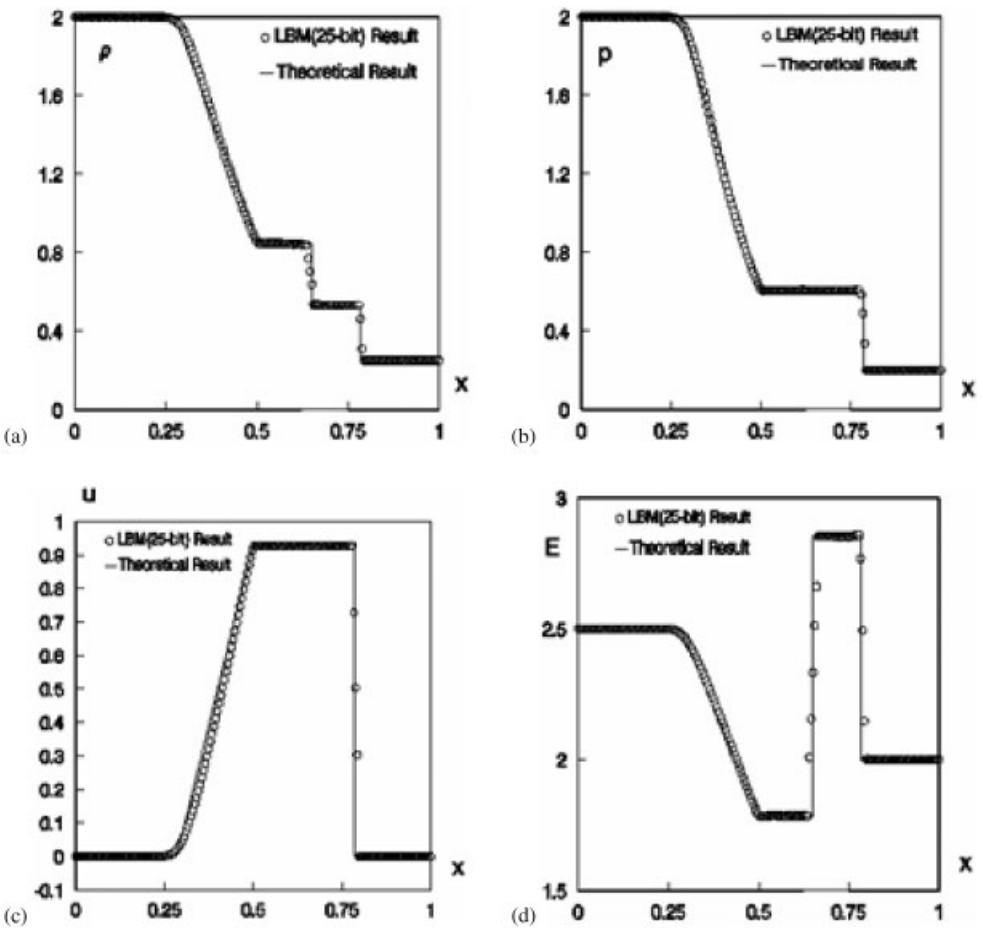

Figure 3. Comparison of exact solution and two-order LBM results of one-dimensional Sod's problem. (a)–(d) (solid lines are exact solutions, circles are LBM results): (a) density; (b) pressure; (c) velocity; and (d) internal energy. Parameters: $\gamma = 1.4$, $c = 3.0$, $\tau = 1.51$, $\varepsilon_A = 2c^2$, $\varepsilon_B = 0.6c^2$, $\varepsilon_D = 0.13c^2$, lattice size 200×4, time $t = 100\Delta t$.

DOI: 10.1002/fld

3. NUMERICAL EXAMPLES

In this section, we apply the LBM to two gas flows. The first one is the typical Riemann problem, namely the shock tube problem of Sod. The second one is a two-dimensional supersonic flow, 4 Mach number incoming flow around a circular cylinder.

3.1. One-dimensional Sod's problem

In order to compute one-dimensional Sod's problem using two-dimensional lattice, we change the initial condition of the typical Sod's problem [15] into the next form.

$$\begin{aligned}(\rho, u, p) &= (2.0, 0.0, 2.0) \quad \text{if } 0 \leqslant x \leqslant 0.5 \\ (\rho, u, p) &= (0.25, 0.0, 0.2) \quad \text{if } 0.5 < x \leqslant 1.0\end{aligned} \tag{78}$$

We use 200×4 grids to simulate the one-dimensional Sod's problem. We select the summation of the second row and the third row as the shock tube, therefore, the density and pressure need to be multiplied by 2.

The comparisons between one-order model and two-order model results are plotted in Figure 2 (for one-order model in Reference [15]) and Figure 3 (for two-order model in this paper). In Figures 2 and 3, we plotted the comparisons between LBM and exact results apart. They show that the two-order model (25-bit model in this paper) has higher accuracy and resolution than the one-order model. They are: (1) the widths of the shock waves are about three to four cells less than the corresponding one-order model; (2) the errors at contact discontinuities appearing in the one-order model have been eliminated; (3) the non-physical oscillation in the front of shock wave has weakened. Table I shows the L_1 norm errors in our LBM and other schemes. We found that the two-order model is more accurate than the one-order model.

Figure 2(a)–(d) displays the results of the density ρ, pressure p, velocity u and the internal energy E calculated by using one-order LBM at the time $t = 100\Delta t$. The boundary condition at the two ends is the Dirichlet condition, at the upper (the fourth row) and under (the first row) boundary condition is the Von Neumann condition. The internal energy E can be calculated by

Table I. The L_1 norm errors of the Sod's problem.

	Density	Velocity	Pressure
The L_1 norm errors of the Sod's problem at $t = 0.1644$			
LBM (25-bit)	0.00521	0.00852	0.00376
LBM (Reference [15])	0.00804	0.01673	0.00792
LAX	0.01769	0.02814	0.01582
ORD	0.00578	0.00959	0.00460
ULT1	0.00437	0.00820	0.00362
STG2	0.00297	0.00494	0.00228
STGU	0.00291	0.00403	0.00216
STGC	0.00172	0.00278	0.00153
ULTC	0.00361	0.00804	0.00362
ROE	0.00836	0.01145	0.00666

These results are from Reference [34], except two LBM results. Lattice size: $N_x = 200$, $t = 0.1644$. The underlined results indicate the smallest L_1 norm errors in every column.

DOI: 10.1002/fld

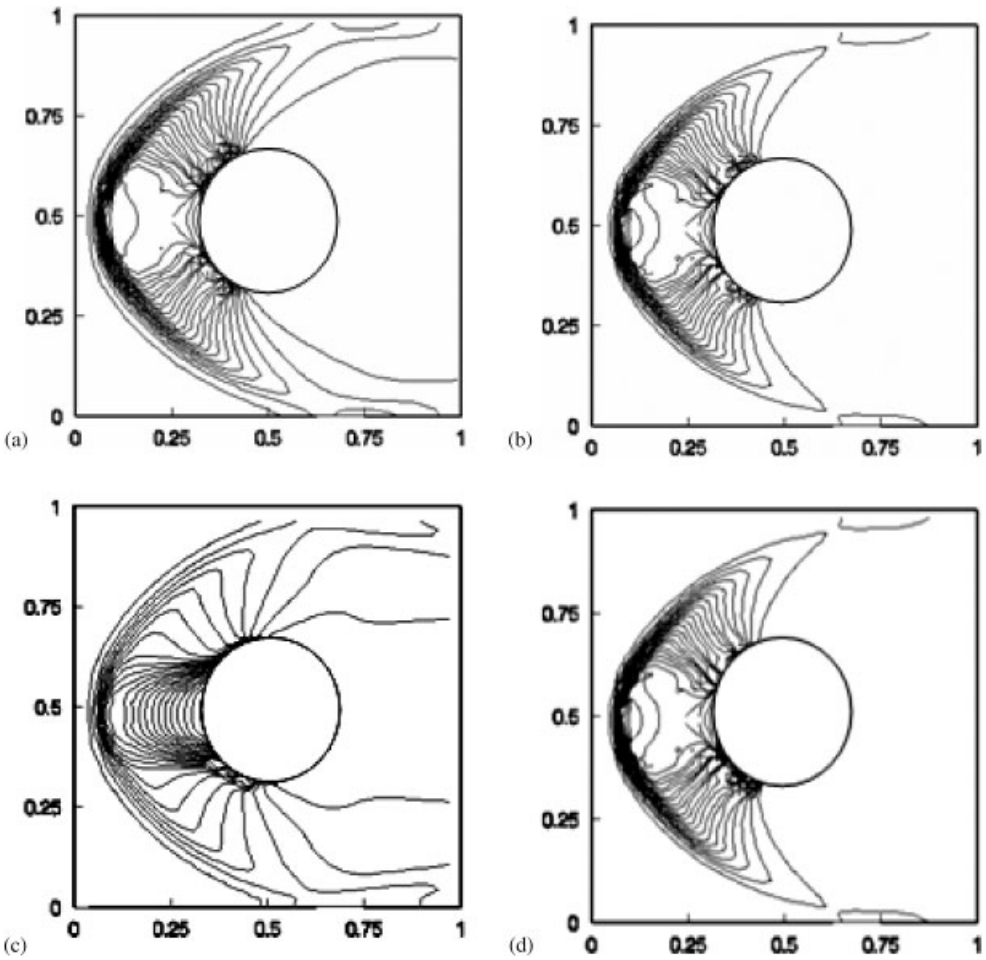

Figure 4. Numerical result of 4 Mach number incoming flow around a circular cylinder: (a) is the density contours; (b) is the pressure contours; (c) the stream lines; and (d) energy ρE contours. Parameters: $\gamma = 1.4$, $c = 3.0$, $\tau = 1.51$, $\varepsilon_A = 2c^2$, $\varepsilon_B = 0.6c^2$, $\varepsilon_D = 0.13c^2$, lattice size 100×100, time $t = 200\Delta t$, $Ma = 4$, $Re = 1000$, line numbers $= 30$.

$E = p/\rho(\gamma - 1)$. Figure 3(a)–(d) displays the results of the density ρ, pressure p, velocity u and the internal energy E calculated by using two-order LBM at the time $t = 100\Delta t$. The boundary condition is the same as Figure 2.

3.2. Flow around a circular cylinder at Mach number 4 [*35*]

The solution domain $[0, 1] \times [0, 1]$ is divided into 100×100 uniform lattice. The circular cylinder is a circle of radius 0.15 and centre at (0.5, 0.5). The initial conditions are $\rho = 1.4$, $u = 4.0$, $v = 0.0$, and $p = 1.0$, thus, incoming Mach number is $M_\infty = 4$, $\gamma = 1.4$. The inlet, upper and bottom conditions are the same as initial conditions. The downstream condition is the Von Neumann

DOI: 10.1002/fld

Table II. The L_1 norm errors of the flows around a circular cylinder with 4 Mach number incoming at line $x = 0.25$.

	Density	Velocity	Pressure
The L_1 norm errors at line $x = 0.25$.			
LBM (25-bit)	0.0371	0.0352	0.00629
LBM (Reference [15])	0.0874	0.0873	0.01254
FSEM (Reference [35])	0.0136	0.0102	0.00277

Lattice size $= 100 \times 100$, $t = 200\Delta t$, $Re = 1000$.

condition, i.e. $\partial F/\partial n = 0$, where F denotes ρ, u, v, and p; n is the vector in the normal direction. The surface of the circular cylinder is the viscous boundary condition, say, $u = v = 0$. In this paper, this model possesses viscosity. From Equation (75), the Reynolds number is $Re = \rho LU/\xi$, where L is the characteristic length ($L = 1.0$), U is the characteristic incoming velocity ($U = 4.0$), therefore, we can select the relaxation factor to design the Reynolds number $Re = 1000$ with $E = p/(\gamma - 1)\rho = 1.78571$, $\tau = \frac{1}{2} + LU/Re(\gamma - 1)kE$. In Figure 4, we plotted four pictures to describe the shock waves at time $200\Delta t$. These are: (a) is the density contours; (b) is the pressure contours; (c) is the stream lines; and (d) is the potential energy contours. It is easy to find shock waves in figures. In order to compare these numerical results with other numerical results obtained by other methods, we select the first-order lattice Boltzmann model in Reference [15] and the finite spectral ENO method (FSEM) in Reference [35] as reference models. Table II shows the L_1 norm errors at line $x = 0.25$ in our lattice Boltzmann model and other schemes. We found this two-order model is more accurate than the one-order model. We also found some large gradient area oscillation in these contour lines. We found that one of the reasons is the poor accuracy of the boundary treatments; we use the lattice to build the boundary of the circular cylinder. Because this flow is supersonic flow, the boundary treatment does not disturb the shock waves. These numerical results show that this second-order model is more accurate than the one-order model in Reference [15].

4. CONCLUDING REMARKS

It is necessary to define total energy and internal energy for the recovery of energy equation. In some papers [13–17], the defined total energy is the total kinetic energy of particles $E_T = \sum f_\alpha c^2/2$, which corresponds to $\varepsilon_A = \varepsilon_B = \frac{1}{2}$, $\varepsilon_D = 0$. This definition completely coincides with the physical concepts of perfect gas, but in one or two-speed model it brings us two difficult problems: (i) it leads to $\gamma = 2$ (so-called Ideal Case [11]); (ii) the energy conservation can be derived from momentum flux conditions. Using multi-speed model and introducing the concept of energy level, we have solved these two problems. In our paper, all equations of perfect gas are successfully included in the lattice Boltzmann model (LBM), and the ratio of specific heats appears as a chosen parameter (so-called General Case).

In order to improve the accuracy of the model, we put an additional term $\rho u_i u_j u_k e_{\alpha i} e_{\alpha j} e_{\alpha k}$ in the equilibrium distribution functions. In order to remove the term $\partial^2 \rho u_i u_j u_k / \partial x_j \partial x_k$, as an essential step, the local equilibrium distribution must satisfy conservation conditions and conditions of higher-order moment equations (5)–(11), thus, we have to use 25 distribution functions to meet

DOI: 10.1002/fld

these higher-order moment equations. In this paper, the Navier–Stokes equations with two-order accuracy are obtained, especially the two-order accuracy energy equation is recovered by defining the moment R_{ij}^0.

There are some problems that need to be solved (1) the stability, numerical dissipation and numerical dispersion to this model, and relations between these numerical phenomena and those parameters need to be solved; (2) the superior limit of the Mach numbers the model can simulate need to be known; (3) we need to study the viscosity and heat transfer phenomena to determine their correctness; (4) some more details on numerical simulations for the boundary condition on the wall, dissymmetrical flows, and flows with higher Mach numbers. We will discuss these problems in further papers.

Finally, we point out that an important problem needs to be solved that is whether to construct higher-order accuracy LBM for the Euler equations or the Navier–Stokes equations.

ACKNOWLEDGEMENTS

This work is supported by 985 Project of Jilin University, the National Nature Science Foundation of China (Grant No. 10072023, Grant No. 90305013), and the Chuangxin Foundation of Jilin University (No. 2004CX041). We would like to thank Prof. Qian Yuehong, Prof. Wang Jianping and Dr Yang Hua for their many helpful suggestions.

REFERENCES

1. Frisch U, Hasslacher B, Pomeau Y. Lattice gas automata for the Navier–Stokes equations. *Physical Review Letters* 1986; **56**:1505–1508.
2. Chen SY, Doolen GD. Lattice Boltzmann method for fluid flows. *Annual Review of Fluid Mechanics* 1998; **3**:314–322.
3. Qian YH, d'Humieres D, Lallemand P. Lattice BGK model for Navier–Stokes equations. *Europhysics Letters* 1992; **17**(6):479–484.
4. Chen HD, Chen SY, Matthaeus MH. Recovery of the Navier–Stokes equations using a Lattice Boltzmann gas method. *Physical Review A* 1992; **45**:5339–5342.
5. Benzi R, Succi S, Vergassola M. The Lattice Boltzmann equations: theory and applications. *Physics Reports* 1992; **222**:147–197.
6. Yan GW. A lattice Boltzmann equation for waves. *Journal of Computational Physics* 2000; **161**:61–69.
7. Yan GW, Song M. Recovery of the solitons using a lattice Boltzmann model. *Chinese Physics Letters* 1999; **16**:109–110.
8. Yan GW, Yuan L. Lattice Bhatnagar–Gross–Krook model for the Lorenz attractor. *Physica D* 2001; **154**:43–50.
9. Versteeg HK, Malalasekera W. An introduction to computational fluid dynamics—the finite volume method. Longman: New York, 1995.
10. Harten A. On a class of high resolution total variation stable finite difference schemes. *SIAM Journal on Numerical Analysis* 1984; **21**:1–23.
11. Harten A, Engquist B, Osher S, Chakravathy R. Uniformly high order accurate essentially non-oscillatory schemes, III. *Journal of Computational Physics* 1997; **131**:3–47.
12. Zhang LT, Wagner GJ, Liu WK. A parallelized meshfree method with boundary enrichment for large-scale CFD. *Journal of Computational Physics* 2002; **176**:483–506.
13. Sethian JA. Theory, algorithms, and applications of level set methods for propagating interface. *Acta Numerica*. Cambridge University Press: Cambridge, U.K., 1995.
14. Woodward P, Colella P. The numerical simulations of two-dimensional fluid flow with strong shocks. *Journal of Computational Physics* 1984; **54**:115–174.
15. Yan GW, Chen YS, Hu SX. Simple lattice Boltzmann model for simulating flows with shock wave. *Physical Review E* 1999; **59**:454–459.
16. Alexander FJ, Chen H, Chen S *et al.* Lattice Boltzmann model for compressible fluids. *Physical Review A* 1992; **46**:1967–1970.

DOI: 10.1002/fld

17. Nadiga BT. An Euler solver based on locally adaptive discrete velocities. *Journal of Statistical Physics* 1995; **81**:129–146.
18. Huang J, Xu F, Vallieres M *et al.* A thermal LBGK model for large density and temperature difference. *International Journal of Modern Physics C* 1997; **8**:827–841.
19. Prendergast KH, Xu K. Numerical hydrodynamics from gas-kinetic theory. *Journal of Computational Physics* 1993; **109**:53–66.
20. Kim C, Xu K, Martinelli L *et al.* Analysis and implementation of the gas kinetic BGK scheme for computing inhomogeneous fluid behavior. *International Journal for Numerical Methods in Fluids* 1997; **25**:21–49.
21. Kotelnikov AD, Montgomery DC. A kinetic method for computing inhomogeneous fluid behavior. *Journal of Computational Physics* 1997; **134**:364–388.
22. Renda A, Bella G, Succi S *et al.* Thermo hydrodynamics lattice BGK schemes with non-perturbative equilibrium. *Europhysics Letters* 1998; **41**:279–283.
23. Vahala G, Pavlo P, Vahala L *et al.* Thermal lattice Boltzmann models (TLBM) for compressible flows. *International Journal of Modern Physics C* 1998; **9**:1247–1261.
24. Sun CH. Lattice–Boltzmann model for high speed flows. *Physical Review E* 1998; **58**:7283–7287.
25. De Cicco M, Succi S, Balla G. Nonlinear stability of compressible thermal lattice BGK model. *SIAM Journal on Scientific Computing* 1999; **21**:366–377.
26. Mason RJ. A compressible lattice Boltzmann model. *Bulletin of the American Physical Society* 2000; **45**:168–170.
27. Mason RJ. A multi-speed compressible lattice Boltzmann model. *Journal of Statistical Physics* 2002; **107**:385–400.
28. Yan GW, Dong YF, Liu YH. An implicit Lagrangian lattice Boltzmann method for the compressible flows. *International Journal for Numerical Methods in Fluids* 2006; **51**(12):1407–1418.
29. Kataoka T, Tsutahara M. Lattice Boltzmann method for the compressible Euler equations. *Physial Review E* 2004; **69**(5):056702.
30. Kataoka T, Tsutahara M. Lattice Boltzmann method for the compressible Navier–Stokes equations with flexible specific-heat ratio. *Physical Review E* 2004; **69**(3):035701.
31. McNamara G, Garcia L, Alder B. Stabilization of thermal lattice Boltzmann models. *Journal of Statistical Physics* 1995; **81**:395–408.
32. Wolfram S. Cellular automaton fluids 1: Basic theory. *Journal of Statistical Physics* 1986; **45**(3/4):471–518.
33. Chapman S, Cowling TG. *The Mathematical Theory of Non-uniform Gas*. Cambridge University Press: Cambridge, 1939.
34. Nessyahu H, Tadmor E. Non-oscillatory central differencing for hyperbolic conservation laws. *Journal of Computational Physics* 1990; **87**:408–419.
35. Wang JP, Qiu QH, Ogawa S. Numerical simulation of viscous supersonic flows by finite spectral ENO method. *Computational Fluid Dynamics Journal* 2004; **12**:191–197.

DOI: 10.1002/fld